Hindawi
Geofluids
Volume 2022, Article ID 9275688, 14 pages
https://doi.org/10.1155/2022/9275688

Research Article

CO_2 Adhesion Characteristics on Solid Surfaces under CO_2 Geologic Sequestration Environment

Jingyue Sun,[1] **Haopo Xu**,[1] **Cong Chen**,[1,2] **Tonglai Li**,[3] **Weizhong Li**,[1,2] **and Yan Qin**[1,2]

[1]*School of Energy and Power Engineering, Dalian University of Technology, Dalian 116024, China*
[2]*Key Laboratory of Ocean Energy Utilization and Energy Conservation of Ministry of Education, Dalian 116024, China*
[3]*Beijing Aerospace Propulsion Institute, Beijing 100012, China*

Correspondence should be addressed to Yan Qin; qinyan_echo@dlut.edu.cn

Received 9 October 2021; Revised 11 January 2022; Accepted 22 January 2022; Published 25 February 2022

Academic Editor: Jinze Xu

Wettability at mineral-CO_2 interface in CGS (carbon geosequestration) is a key parameter for risk assessments and storage capacity estimations. Many studies of wettability achieved inconsistent results, while adhesion could be a potential mechanism causing huge wettability alteration. CO_2 adhesion characteristics have been revealed for CO_2/brine/mica system under a wide range of pressures, temperatures, and salinities by analyzing static and dynamic contact angles. Under all experiment conditions, the average static CA ranges from 19.5° to 32.1°. In 8 MPa experiments, CA decreases from 26.0° to 19.5° with the increasing salinity. Similar trends were also observed under 12 MPa condition. However, CA does not show clear dependence on pressure. A concentric probe was designed by which vertical position of the probe can be changed by rotating the screw of the probe holder while horizontal degrees of freedom are restricted. With this concentric probe, contact angles were obtained at different positions of the same sample to investigate the effect of heterogeneity of sample surface. Uncertainty and large hysteresis of dynamic contact angles were found which related with measurement positions. These large hystereses as obvious sign of adhesion had good repeatability at specific surface positions. Further electron microscope test demonstrated the correlation between large hysteresis and smoother surfaces which is consistent with the DLVO theory-based water film thickness hypothesis on adhesion. This study enriched the data on the wettability of mica and may shed light on CO_2 adhesion on solid surfaces for better understanding the fate of CO_2 during sequestration.

1. Introduction

The massive burning of fossil fuels and emission of large amounts of greenhouse gas into the atmosphere have caused serious greenhouse effects and environmental problems. However, nowadays the demand for fossil fuels is huge and mitigating anthropogenic CO_2 emission from the source is necessary. CGS (carbon geosequestration) technology in which CO_2 is captured from main emitters and injected into underground geological formations is currently regarded as an effective solution to the greenhouse effect [1–3]. The injected geological formations can be deep saline aquifers [4], depleted oil/gas fields [5], and deep coal mines [6–8] where CO_2 is trapped by means of four mechanisms: structural [9, 10], residual [11–14], solubility [15, 16], and mineral trapping [17]. Structural and residual trapping are the two most important storage mechanisms in the short term, and capillary pressure plays a crucial role to resist CO_2 plume upward migration [18, 19] and trap disconnected CO_2 bubbles between water in rock formation pores after drainage and imbibition processes [20]. Wettability is a key factor impacting the magnitude and direction of the capillary force and is usually quantified by contact angle (CA). Wettability of caprocks in CO_2-brine systems is a key parameter of structural trapping influencing the efficiency and safety of sequestration [21, 22].

As representative of clay minerals, mica was usually selected to characterize wettability of caprocks under CGS condition in previous research in which CA was measured [23–28]. Chiquet et al. [25] found that the CA increased

significantly with pressure and mica exhibited hydrophobicity under high pressure. As ion concentration increased from 0.1 M to 1 M, the hysteresis of dynamic CA increased by about 25°. Broseta et al. [24] reported that θ_A increased more than 30° with pressure showing hydrophobicity as pressure increased from 5 to 140 bar, and the receding CA θ_R increased slightly (from 28° to 45°). Farokhpoor et al. [26] used stricter cleaning technology and found CA increases from 15° to 36° with increasing pressure from 1 MPa to 30 MPa. They also reported increased CA with reaction time of a CO_2 droplet in contact with mica (θ =35–61° from 0 to 48 days under 105 bar, 36°C). Wang et al. [29] measured CA in CO_2-brine-phlogopite system and reported lower and nearly constant CA: $\theta_R = 20°$ and $\theta_A = 20–43°$. Wan et al. [27] found that reaction with water-saturated supercritical CO_2 phase severely roughened the muscovite surfaces and largely increased CA hysteresis. Reproducibility of dynamic tests was poor. Using the pendant drop technique, Arif et al. [30] found that both θ_A and θ_R increased with pressure and salinity, but decreased with temperature. Reported data are divergent, from strongly water-wet to even CO_2-wet, with inconsistent trends of pressure and salinity. Wan et al. [27] identified several possible common causes: (1) starting substrates of nominally same composition can have very different intrinsic surface chemical properties and reactivity, variably altered surface chemistry resulting from cleaning methods, or different initial surface roughness; (2) different types and amounts of contaminants; (3) phase disequilibrium induced CO_2 droplet dissolution; and (4) CO_2 and substrate contact time, procedures, and repetition may affect water film or CO_2 stability on the substrate.

However, research on the effect of adhesion on wettability in CO_2-brine-mica system is insufficient and adhesion may account for discrepancy in CA measurements. Some special phenomena have been discovered in previous studies on wettability of mica. Chiquet et al. [25] described wettability alteration caused by contact line pinning or wettability hysteresis, and Jafari and Jung [31] also reported decrease in wettability by time due to heterogeneity and pinning effect of triple line. The pinned contact line represents a high energy barrier locally [32]. Carre and Lacarriere [33] indicated that interfacial adhesion could be the mechanism underlying or contributing to both pinning and hysteresis. Adhesion usually describes the molecular affinity of different surfaces at the nanometer level, usually occurs on extremely smooth surfaces and greatly alters the wettability. Moreover, adhesion tests of CA measurements have long been applied in research of petroleum reservoirs. Using DLVO theory (Derjaguin, Landau, Verwey, and Overbeek), stability of water films has been predicted in mineral-water-oil systems which is of significant impact to wettability [34–36]. DLVO model calculations and measurements of brine films on mica confined by $scCO_2$ indicate that water film thicknesses of several nm are stable [37]. Based on DLVO theory, Wang et al. [29] proposed adhesion tests controlling parameters (surface roughness, CO_2 partial pressure, and pH) related to water film thickness and consistent experimental results were obtained.

Because of experimental limitations, there are many uncontrollable factors accounting for test diverge, such as variable procedures for different researchers and surface heterogeneity. In this study, we emphasized on repeated tests under consistent conditions in CO_2-brine-mica system; in this way, wettability can be analyzed with fewer influencing factors (such as pressure, temperature, and salinity). Irregular contact lines and wettability changes are common features of adhesion, so analysis of these possible phenomena can reveal clues to adhesion.

The experimental device and measuring method of CA will be introduced in Section 2 of this paper. In Section 3.1, the influence of pressure, temperature, and salinity on the static wettability of phlogopite will be analyzed and the movement characteristics of the bubbles in the static CA process will be explored. The dynamic contact angle and various factors affecting dynamic wettability will be analyzed in Section 3.2, and electron microscope and EDS tests will be introduced in Section 3.3. Finally, this research will be summarized at the end of this article.

2. Experimental Methods

Muscovite, as one kind of common mica, was selected for the analysis as it is a primary mineral of shales. Muscovite and phlogopite mica have been used in contact angle experiment. Muscovite of v1 grade was provided by Electron Microscopy Sciences. As the highest quality mica provided, the muscovite mica is clear, hard, of uniform color, nearly flat, and free of all stains, cracks, and other similar defects. Phlogopite was produced in Lingshou County, Hebei. Pure CO_2 (99.99%) was provided by Dalian Airichem Specialty Gases and Chemical Co., Ltd. Distilled water provided by Watsons, and 99.5% AR NaCl was used to configure saline solution. Distilled water was also used during the cleaning process. Freshly cleaved muscovite sheets are easy to be contaminated by impurities due to negatively charged surface, so attention was paid to avoid contact with noncleaning liquid substances. Once cleaved, the thin sheet was thoroughly cleaned with ethanol and distilled water with clean hand gloves, dried, and immediately sent into the reaction chamber (for CA measurement). A similar cleaning process was also adopted in silica and mica CA tests [27, 31, 38].

The whole experimental procedure is shown in Figure 1. In the preparation phase, CO_2 was compressed into the high-pressure tank acted as CO_2 source, whose pressure was higher than the experimental value to supply CO_2 for subsequent equipment thorough the pressure reducing valve and check valve. Brine solution and CO_2 were pre-equilibrated in a high-pressure stirred tank under scheduled conditions for at least 24 h. A high-pressure reaction chamber with two parallel visible glasses was designed for CA measurement. The chamber contains an internal groove for placing samples on the upper side. The chamber is also wrapped outside with an electric heater connecting to a thermocouple for temperature control and inside equipped with a pressure detector. At the experiment beginning, once the muscovite sheet was placed, the reaction chamber was heated to the target temperature and valves 3, 11, and 12

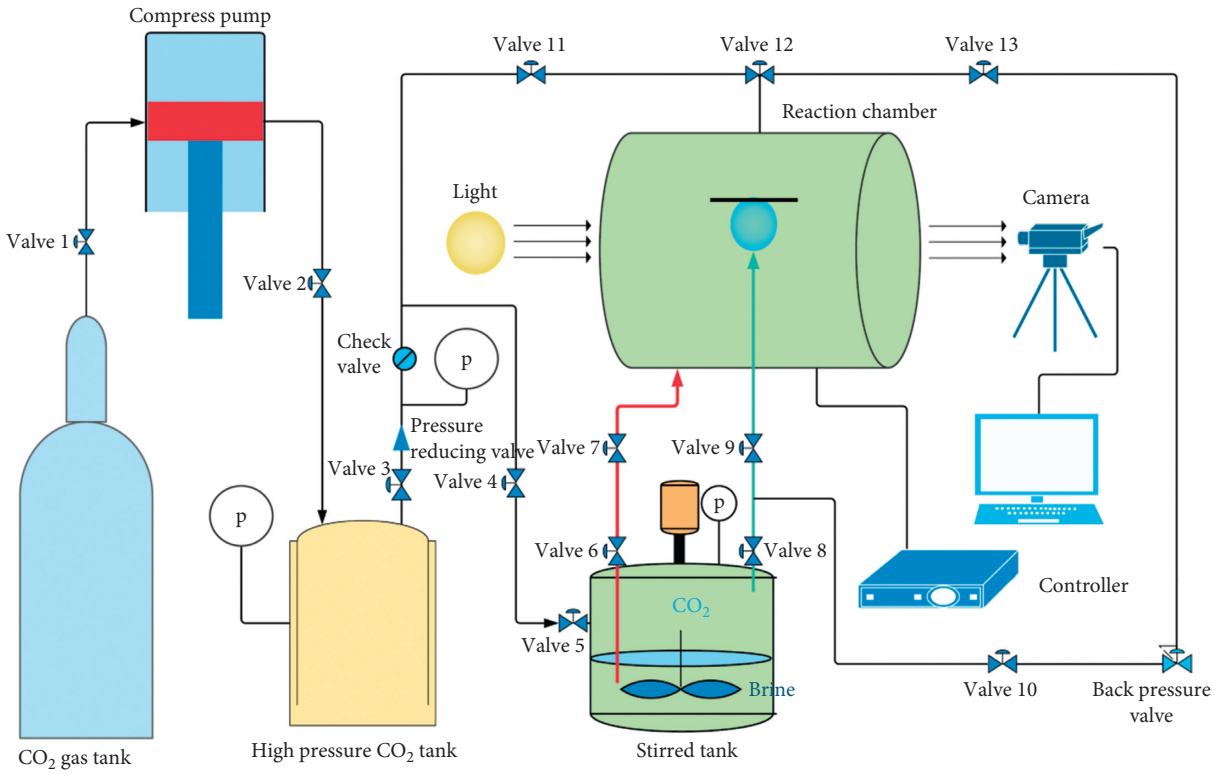

FIGURE 1: An illustration of the experimental procedure. CO_2 bubbles and brine used for CA measurements were provided by the stirred tank with over 24 h balance, so the influence of dissolution can be negligible.

were opened to charge CO_2 to target pressure. The pressure of stirred tank was a little higher than that of the reaction chamber to inject balanced brine and CO_2. As the chamber got the target temperature, valves 6 and 7 were slightly opened to slowly inject brine until brine immersed the muscovite sheet and excess CO_2 in the chamber was released from the back pressure valve. After injection, the whole system would still be balanced for 3 h before measurement.

At the down side of the reaction chamber, there is a height-adjustable needle holder which can install concentric or eccentric probes. Equipped with a concentric probe, the vertical position of the probe can be changed by rotating the screw of the probe holder, while horizontal degrees of freedom are restricted. Equipped with an eccentric probe, the probe does a circular motion; thus, CA can be obtained at different positions of the sample and four positions were marked as shown in Figure 2. Since the probe base and the device are threaded, the height of the probe will change during rotating. In the four marked positions, position ① is furthest to the muscovite surface while position ④ is the nearest. Distances to the muscovite surface for positions ①, ②, ③, and ④ are 3.6, 3.2, 2.8, and 2.4 mm, respectively. In previous CA experimental studies, only concentric probes were adopted, while dynamic CA results were affected by chemical heterogeneity and dynamic CA results of only one position of the sample can be obtained. Concentric probes can examine wettability of multiple locations on the sample to analyze CA with chemical heterogeneity.

The captive drop method was used for CA measurement. In static CA measurements, valves 8, 12, and 13 were opened and a balanced CO_2 bubble from the stirred tank was released from the probe by controlling valve 9 and hit the mica surface due to buoyancy force. After the system reached balance, the three-phase contact angle presented was static CA. Dynamic CA tests contain two stages: (1) like static tests, opening valves 8, 12, and 13, the probe slowly released a CO_2 bubble near the surface and the bubble gradually expanded on the surface of the mica. CA when the CO_2 contact line was constantly growing during the CO_2 driving brine process was called θ_R (receding CA); (2) opening valve 10, closing valves 8, 12, and 13, and reducing the backing pressure valve, the probe slowly absorbed CO_2 by controlling valve 9 and CO_2 bubble gradually shrunk on the mica surface. CA when the CO_2 contact line constantly decreased during the brine driving CO_2 process was called θ_A (advancing CA). For convenience, all CAs in this study are referred in water phase. Furthermore, advancing CA measurements can be separated into two periods. In the first period, the CO_2 bubbles started shrinking and CA increased continuously but the contact line did not move. In the second period, the contact line started to decrease while CA maintained a relatively constant value. Angles obtained in the second period were called θ_A. CA images were taken by using Canon EOS 500d. Images were processed through ADSA (Axisymmetric Drop Shape Analysis), an analysis plugin integrated in ImageJ [39]. The plugin proposed by Potentbery is based on Laplace equation to calculate the key

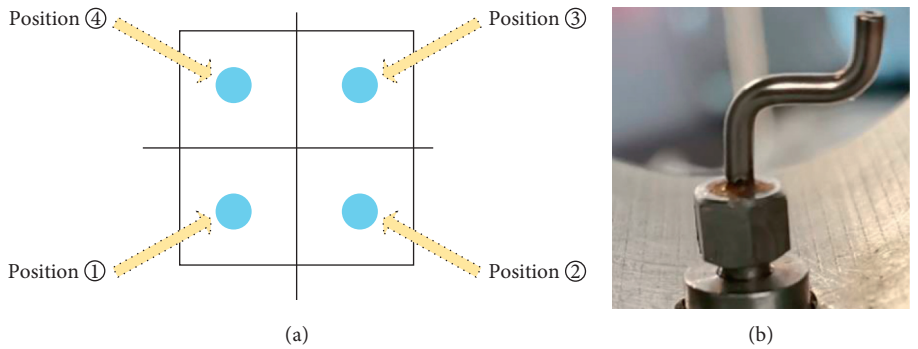

Figure 2: (a) Four marked positions for dynamic tests. (b) Eccentric probe with threaded connection to base.

point curvature of the symmetric droplet interface and interfacial tension by which CAs were calculated.

3. Results and Discussion

3.1. Static Contact Angles. The influence of pressure and temperature changes on the static wettability of phlogopite is shown in Figure 3. Static CA angle increased with temperature in the range of 45–80°C, while the influence of pressure was unclear. Phlogopite exhibits hydrophilicity under all measurement conditions ranging from 19° to 40°. The impact of temperature is consistent with Farokhpoor et al. [26] and Saraji et al. [40] in CO_2/quartz/brine system, while Arif et al. [30] obtained opposite results. Influence of salinity on phlogopite surface was also investigated under various pressures and is shown in Figure 4. Static CA increased with salt concentration at phlogopite surface. Impact of $MgCl_2$ and NaCl on wettability was similar expect the condition of 0.31 mol/L $MgCl_2$ which showed larger CA (up to 38°) under 8–12 MPa. Impact of salinity can be explained by variations in zeta potentials (high negative values under low salinities to low negative values under high salinities) [41, 42] causing less polar surfaces and higher CA.

The static CA results of muscovite are summarized in Table 1. Under all conditions, the average static CA ranges from 19.5° to 32.1°. In 8 MPa experiments, CA decreases from 26.0° to 19.5° with the increasing salinity. Similar trends were also observed under 12 MPa condition. However, CA does not show clear dependence on pressure. Multiple sets of repeatability experiments were conducted in 12 MPa, 45°C, and 1 mol/L NaCl brine, and the results are summarized in Table 2. For each set of experiments, individual mica sample was used. Average CA of each set ranges from 18.5° to 29.1°. In sets 6 and 8, bubbles with larger static CA (32.8° and 34.0°) were observed.

Wang et al. [28] obtained similar static results in CO_2-brine-phlogopite system. Wan et al. [27] obtained scattered CA data using the captive CO_2 droplet method (20–80°) comparing to the water-droplet method (30–47°); under the same method, both value and scatter of our static results are low.

The static CA of most bubbles is the same on the left and the right side, while under both pressures (8 and 12 MPa), we observed abnormal bubbles shown in Figure 5 with unequal

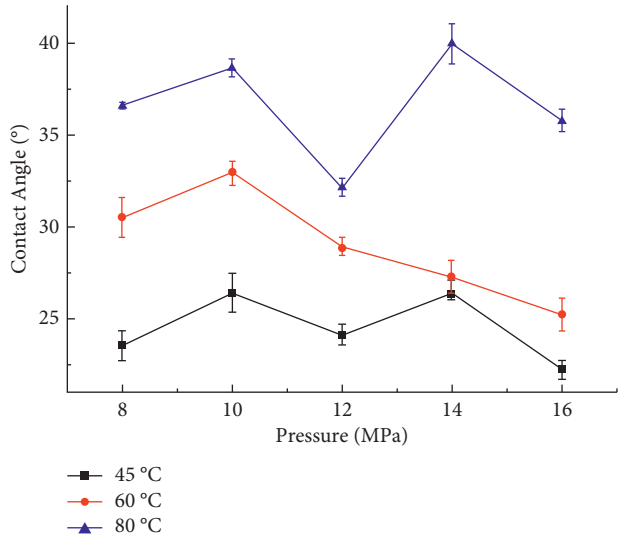

Figure 3: Phlogopite static CA results with pressure and temperature change at 1 mol/L NaCl.

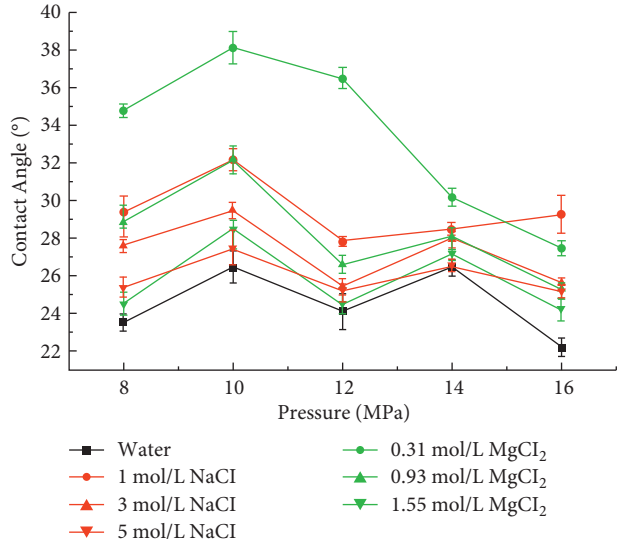

Figure 4: Phlogopite static CA results with pressure and salinity at 45°C.

Table 1: Muscovite static CA results at 5 different conditions and temperature at 45°C.

Condition	Average static CA (°)
8 MPa H_2O	26.0 ± 2.5
12 MPa H_2O	32.1 ± 3.4
8 MPa 1 mol/L NaCl	22.4 ± 3.3
8 MPa 2 mol/L NaCl	19.5 ± 2.0
12 MPa 1 mol/L NaCl	22.1 ± 4.1

CA of both sides. CA differences between the left and the right side were identified as feature for adhesion [28] while such bubbles are rare. In the whole static tests, only if three-phase system entered equilibrium would CA be called static. Once released, a CO_2 bubble floated up, hit the surface, rebounded, and finally attached. This process was dynamic, and surface properties made great difference in determining bubbles' movement. Continuous fluctuation in bubbles' shape was observed at the moment of hit, causing the constantly changing contact line that made the process more like a dynamic CA test.

A high-speed camera was used to further explore the changes in the movement characteristics of the bubbles in the static CA process. Take the process of bubble movement at 60°C, 16 MPa, at phlogopite as an example; captured images showed that the movement of CO_2 bubbles can be divided into three stages: bubble growth, bubble rising, and motion after collision between bubble and mica surface, which are shown in Figures 6–8, respectively. In the final stage, the bubble collided with the mica surface under combined effects of kinetic energy of fluid, surface energy of the gas-liquid interface, and gravitational potential energy of the bubble. Deformation of the bubble was extremely serious, and when it reaches a certain level, the bubble bounced to the opposite direction. The collision-bounce process happened repeatedly until the bubble kinetic energy was exhausted. Finally, the shape of the bubble, the length of the contact line, and the area occupied on the mica surface remained constant. Therefore, discrepancy of static CA of two sides may be similar to the cause of CA hysteresis and influenced by chemical heterogeneity in terms of surface energy states and roughness.

In order to better describe the situation during the bubble rising, velocity of the bubble under various pressures shown in Figure 9 was processed. The velocity at growth stage is almost 0 and rises continuously under buoyancy force once the bubble escapes from the injection probe. Then, the bubble collides with phlogopite surface, velocity decreases, and bubble bounces away from the surface changing the direction of velocity. At the farthest distance from the surface, velocity reaches its minimum value (0), and then the bubble accelerates again under buoyancy force and collides with the mica surface again and again. During repeated collisions, energy is dissipated and fluctuation of velocity becomes smaller and smaller until quiescence. The maximum bubble velocity gradually decreases in the range of 8–14 MPa which can be explained by smaller density difference during pressure rise. The number of collisions also decreases with pressure. Velocity analysis shows the characteristics of bubble movement in the captive drop method to better understand the connection between static and dynamic CA measurements.

3.2. Dynamic Contact Angles. The mutual displacement of brine and CO_2 under geological storage conditions is a dynamic and complex process, and the study of dynamic wettability has an important impact on practical engineering applications. In an ideal three-phase system, the CA should be a constant value as a thermodynamic quantity. However, dynamic experiments found that even on a homogeneous and smooth muscovite surface, the advancing contact angle is usually greater than the receding contact angle, which is often referred to as CA hysteresis [25]. CA hysteresis can be very large, with advancing and receding angles differing by more than 60° and can be due to mechanical or chemical effects [43]: (1) effect of surface roughness, (2) effect of chemical heterogeneity, (3) orientation of surface chemical groups depending on the phase they are exposed to, and (4) interdiffusion and interdigitation.

3.2.1. Repeated Experiments in 12 MPa. Dynamic tests were firstly conducted in 8 MPa which is closing to supercritical pressure with poor reproducibility. Pressure was then set at 12 MPa to avoid instability due to supercritical properties. Eccentric probes were used, and tests were conducted in four marked positions. Eight repeated tests were conducted in 12 MPa, 1 mol/L NaCl, and 45°C, and the results are summarized in Tables 3 and 4. Each set of experiments used the same cleaved sheet of muscovite and was completed within one day to reduce the influence of system reaction. The range of receding CA is similar to that of static CAs, and deviation is relatively small. However, large advancing CA discrepancy (from 24° to 69.5°) was observed. It is hard to say which factor accounted for poor experiment reproducibility, and it is necessary to analyze uncertainties before adhesion, such as surface properties, surface distance, and bubble contraction speed.

A range of receding CAs was close to that of static CA. Receding CA of the last two sets was higher than the other six sets by about 7°. For each set, receding CA of four positions was similar compared to deviations caused by data processing. Despite large deviation of advancing CA, it can be seen that CO_2 bubbles are more likely to remain on the muscovite surface with the longer surface distance from the probe. At position ① farthest from the surface, all the bubbles stayed on the muscovite surface after the test, while at positions ③ and ④ closer to the surface, 3 sets of CO_2 bubbles finally sucked into the probe. Whether CO_2 bubbles finally remained on the surface is also affected by θ_A. In the 7th and 8th experiments where the advancing contact angle is larger, all the bubbles remained on the muscovite surface after the dynamic test, while in the second set, this phenomenon was only observed at position ① where the probe is farthest. Here, we try to avoid using "adhesion" because it was found that the distance of the probe will affect the final state of the CO_2 bubble, but surface distance had no obvious effect on advancing CA. "Adhesion" can only be characterized by the huge change in

Table 2: Muscovite static CA results at 12 MPa, 1 mol/L NaCl, and 45°C.

Sample	Bubble 1 (°)	Bubble 2 (°)	Bubble 3 (°)	Bubble 4 (°)	Average CA (°)
1	22.4	20.6	20.2	19.3	20.8 ± 1.1
2	20.5	19.7	19.9	19.5	19.9 ± 0.4
3	18.8	17.7	18.8	18.5	18.5 ± 0.5
4	19.0	21.5	20.2	18.7	19.9 ± 1.1
5	19.8	20.3	21.2	21.1	20.6 ± 0.3
6	18.2	18.7	20.1	32.8	22.5 ± 6.0
7	24.2	20.8	22.4	25.1	23.1 ± 1.7
8	21.1	22.2	24.5	34.0	25.5 ± 5.1
9	28.5	30.6	30.1	27.3	29.1 ± 1.3

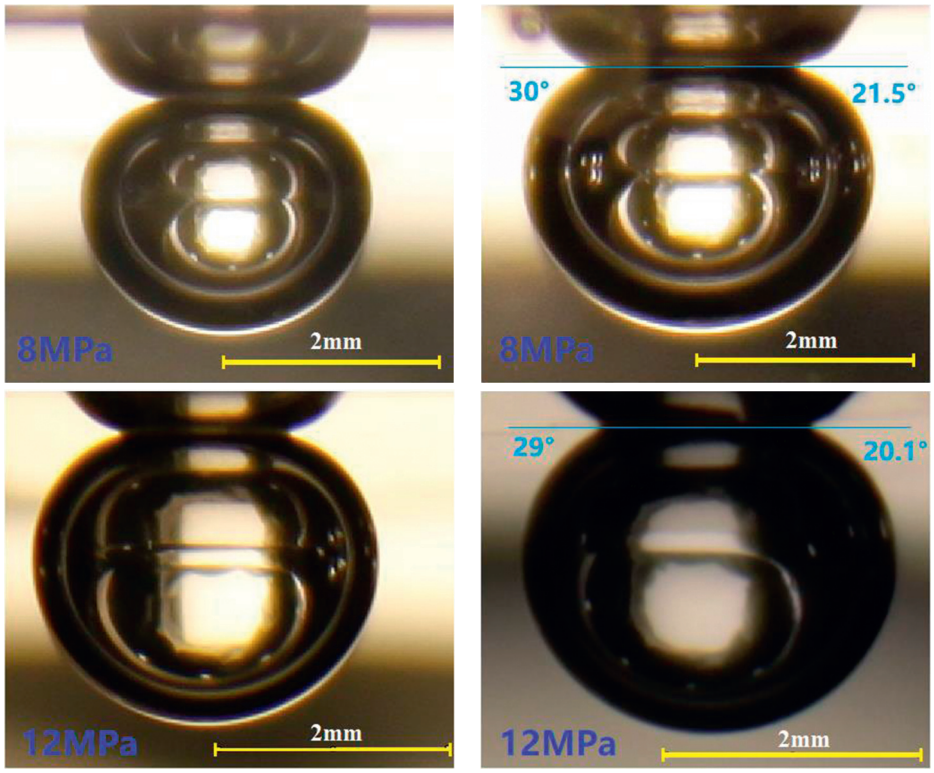

(a) (b)

Figure 5: Static CA experiments at 1 mol/L NaCl and 45°C at muscovite surface. (a) The left two bubbles are symmetrical and could be found in most cases. (b) The right two bubbles have unequal static CA of both sides and are rare.

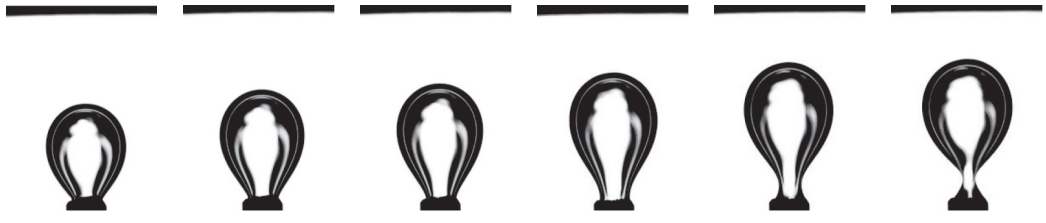

(a) (b) (c) (d) (e) (f)

Figure 6: Schematic diagram of bubble growth. (a) $T = 0$ s. (b) $T = 0.012$ s. (c) $T = 0.036$ s. (d) $T = 0.120$ s. (e) $T = 0.184$ s. (f) $T = 0.196$ s.

wettability as it may cause. According to Laplace pressure balance acting downwards on the surface, the net force parallel to interfacial tension force acting on the rim of the droplet can be expressed by

$$F = \pi D_0 \gamma_{LG} \cos\theta, \quad (1)$$

where D_0 (m) is the diameter of the circle spread by CO_2 bubbles on the muscovite surface, (N/m) is the interfacial

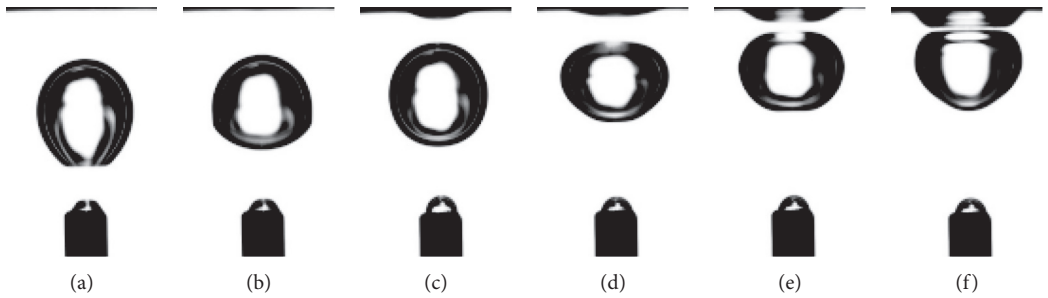

Figure 7: Schematic diagram of bubble rise phase. (a) $T = 0.2$ s. (b) $T = 0.216$ s. (c) $T = 0.228$ s. (d) $T = 0.240$ s. (e) $T = 0.264$ s. (f) $T = 0.272$ s.

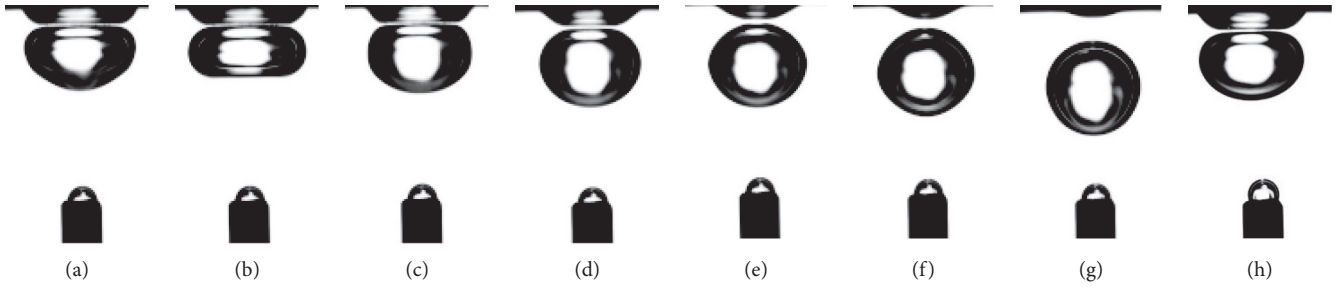

Figure 8: Schematic diagram of motion after collision between bubble and phlogopite surface. (a) $T = 0.276$ s. (b) $T = 0.284$ s. (c) $T = 0.296$ s. (d) $T = 0.304$ s. (e) $T = 0.312$ s. (f) $T = 0.324$ s. (g) $T = 344$ s. (h) $T = 0.500$ s.

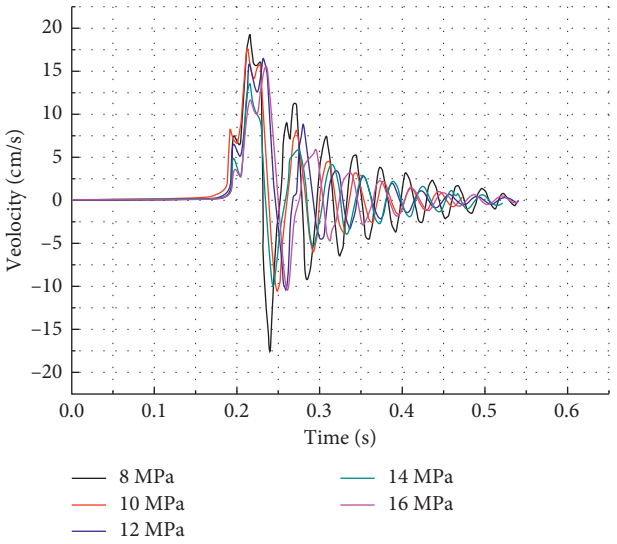

Figure 9: Change of bubble velocity with pressure at 80°C and water at phlogopite surface. The distance between probe and sample is 8.52 mm.

Table 3: Receding CA results of repeated experiments at 12 MPa, 1 mol/L NaCl, and 45°C.

Experiment set	Position ①	Position ②	Position ③	Position ④	Average receding CA (θ_R) (°)
	Receding CA (θ_R) (°)				
1	21.3	18.5	19.8	19.6	19.8 ± 1.0
2	18.2	18.9	18.4	19.7	18.8 ± 0.6
3	18.8	18.9	18.6	18.6	18.7 ± 0.1
4	18.3	18.9	—	19.8	19.0 ± 0.6
5	20.0	19.8	18.2	20.0	19.5 ± 0.8
6	22.0	21.7	20.9	20.9	21.3 ± 0.5
7	27.9	25.0	24.5	26.3	25.9 ± 1.3
8	27.7	26.6	27.1	25.3	26.7 ± 0.9

Table 4: Advancing CA results of repeated experiments at 12 MPa, 1 mol/L NaCl, and 45°C.

Experiment set	Position ①		Position ②		Position ③		Position ④	
	CO_2 remain or not	θ_A (°)	CO_2 remain or not	θ_A (°)	CO_2 remain or not	θ_A (°)	CO_2 remain or not	θ_A (°)
1	Y	41.3	Y	42.0	N	38.4	Y	43.1
2	Y	30.4	N	24.0	N	31.8	N	39.9
3	Y	51.0	Y	37.8	Y	39.6	N	37.1
4	Y	38.1	Y	41.2	Y	-	Y	43.5
5	Y	52.1	Y	51.4	N	45.3	N	40.1
6	Y	50.0	Y	49.6	Y	47.0	Y	56.9
7	Y	68.8	Y	64.3	Y	59.7	Y	60.7
8	Y	63.0	Y	58.7	Y	69.5	Y	56.5

"CO_2 remain or not" means whether CO2 bubbles remain on muscovite after dynamic tests.

tension between CO_2 and brine, and θ (°) is dynamic CA. When θ and interfacial tension between CO_2 and brine are constant value, the force normal to the surface at the three-phase interface is related to the diameter of the bubble spreading on muscovite. When the CO_2 bubble is about to leave the probe, the shape of the bubble connected to the probe is the same with the same θ_A. Closer the distance of probe to muscovite, force needed to drag and detach CO_2 bubble from muscovite surface is smaller. Comparing to results of all sets, θ_A of the second set was generally small, while in the seventh and eighth sets, θ_A was large. Large deviations mainly occurred in different experimental sets. For the same set of experiments, at the four measured positions, θ_A showed no obvious dependence on the probe distance and deviation is relatively small.

A typical dynamic contact angle process is shown in Figure 10. In the dynamic contact angle measurement, the complete displacement process includes two stages: ① bubbles occupy the surface of mica from nothing and ② bubbles occupy the surface of mica to finally be sucked into the probe. A measurement process is equally divided into 15 segments according to time to indicate the change of dynamic contact angle during the process, which is convenient for the comparison of multiple dynamic measurements. In the process of advancing and receding measurement, both sides of CA remain the same. While in some cases, contact line pinning or sudden leap was observed, for example, that happening at position ① at the third set and position ④ at the fifth set, respectively. Dynamic CA and contact line change of these abnormal dynamic advancing processes are shown in Figure 11. In position ① of the third set, CAs of both sides were equal and gradually increased while halfway CA of left side exceeded the right side and reached maximum at about 66°. Movement of three-phase contact point also revealed that, in the final stage, left three-phase point remained stopped until the bubble left the probe. The other abnormal set happened at position ④ of the fifth set. As shown in Figure 12, θ_A of both sides gradually increased and stayed in a range and then θ_A of right side sharply decreased to a very small value causing the rapid separation of bubble from the muscovite. From the movement of three-phase point, we can see that the right three-phase point did little movement in the early stage but suddenly leaped accompanying with sudden decrease of right CA. In the two abnormal sets, it seemed that surface energy barrier acting on

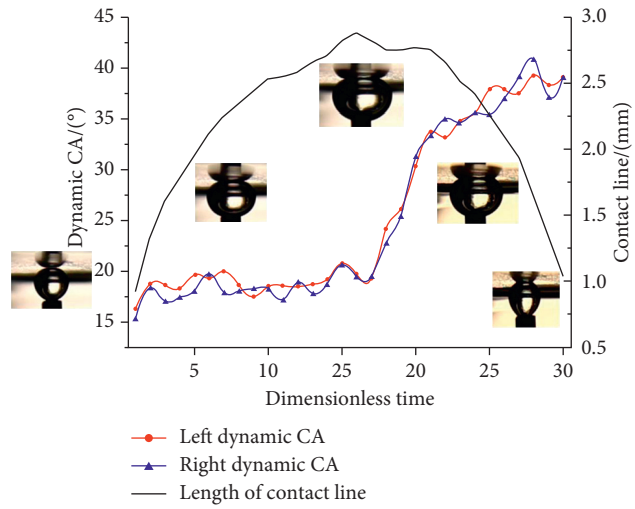

Figure 10: Dynamic CA and contact line change of the whole dynamic process at position ④ in experiment set 3 at 12 MPa, 1 mol/L NaCl, and 45°C. The process was divided into 30 parts by time and exhibited CA hysteresis.

certain part of the bubble occupied area and surface heterogeneity may account for the unusual phenomenon. Huge deviation in θ_A results was related to contact line pinning or leap phenomenon. While contact line pinning and leap were observed at certain position of surface causing dramatically change of θ_A, the conclusion is that the dynamic wettability tested is of poor repeatability, and indeed, there is a certain probability to get large θ_A (phenomenon of adhesion) where the muscovite exhibits intermediate hydrophilicity.

3.2.2. Various Factors Affecting Dynamic Wettability. The fluid flow in the underground storage environment is complicated, and the migration rate of brine and CO_2 varies from place to place due to the pores sizes. Because the probe bubble retracting speed was difficult to be consistent in the experiment, we also verified dynamic characteristics under two contraction rates (slow and fast) at 8 and 12 MPa. To avoid the influence of surface differences and system chemical reaction on the results, experiments were conducted on the same surface and the same position, and the overall timespan did not exceed 0.5 hours. The results are shown in Figure 13. Under both pressures, θ_R was stable. In

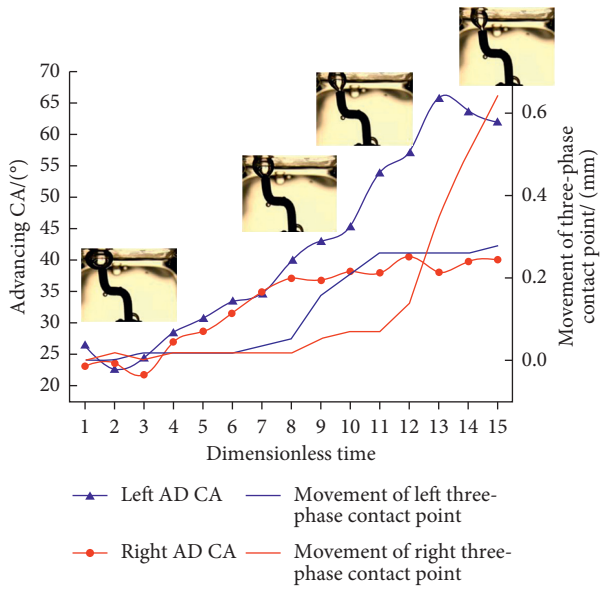

Figure 11: Advancing CA and contact line change at position ① in experiment set 3 at 12 MPa, 1 mol/L NaCl, and 45°C. The whole advancing process was divided into 15 points, and we can see two stages: (1) length of contact line keeps almost unchanged; (2) length of contact line keeps decreasing.

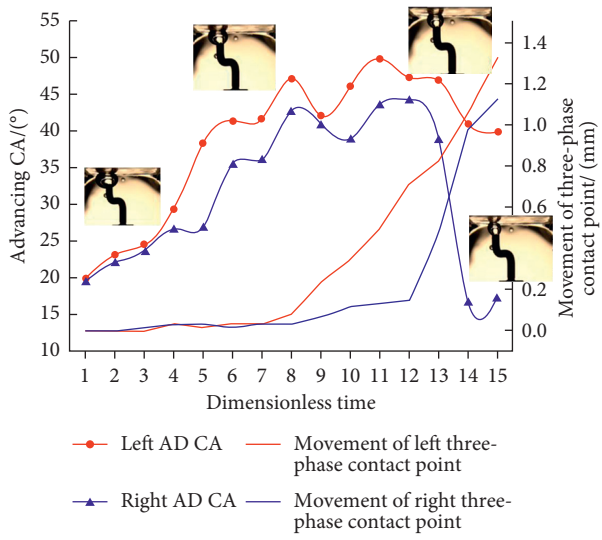

Figure 12: Advancing CA and contact line change at position ④ in experiment set 5 at 12 MPa, 1 mol/L NaCl, and 45°C. The processing method is the same with Figure 8.

8 MPa condition, θ_R has approximately 10° fluctuations while the average value was equal. 12 MPa results were the same showing that contraction rates did not have a huge impact on dynamic characteristics.

Impact on the system chemical reaction was also investigated. Wan et al. [27] proved that long-term exposure in brine severely roughened the muscovite surface leading to large CA hysteresis. The dynamic results showed that θ_A in set 2 was the smallest and that in sets 7 and 8 was the largest, so comparison was focused on these three sets. The dynamic results of set 2 in positions ② and ③ are shown in Figures 14 and 15. At position ②, θ_R in two tests was very close. θ_R in the early test was about 5° larger than θ_R, while in the later test, CA hysteresis was 0° in the final stage. Hysteresis was small in both tests. At position ③, dynamic CA showed similar values. It is interesting to find that processes in right θ_A were exceptionally similar with the suddenly decrease in right θ_A at the final stage. Despite small hysteresis in experiment set 2, difference in the left and right θ_A was found. The results of sets 7 and 8 are shown in Figures 16 and 17. In both sets, values of dynamic results were consistent. The dynamic results showed good reproducibility at the same position; thus, proving the poor reproducibility of whole dynamic tests may be due to factors such as surface heterogeneity rather than artificial experimental operations, system reactions, and contraction rates.

3.3. Electron Microscope and EDS Tests. From the dynamic results, it can be seen that large discrepancy in wettability mainly comes from different experimental groups, that is, different measurement surfaces; even at different positions on the same surface, dynamic wettability still shows certain differences. In order to further clarify the effect of adhesion, we carried out EDS scanning electron microscopy analysis on experimental samples. Muscovite surfaces were cleaved from one 25 mm × 25 mm sample with a thickness of about 0.3 mm. Layered cleavage is complete and extremely smooth, while surface properties may be different. Contamination may also be introduced in the process. Given huge dynamic deviations in sets 4 and 7, electron microscope tests were conducted on the two samples after experiment. A newly cleaved sample was also tested for comparison. Microscope and EDS results are shown in Figures 18–20. Comparing the sample of sets 4 and 7, it is clear that the surface of the former sample surface contains many dotted unknown substances and 10 micron-level floc-like substances were found, closing to which substances seeming to be caused by the curl of the mica skin were also found. While in the sample of set 7, under 10000X magnification, the number of dotted substances was small and no floc-like substances were found. The total surface looks much cleaner and looks smoother than set 4.

It is hard to distinguish these dotted and floc-like substances, and parts of them may be contaminated. Iglauer et al. [44] introduced contamination in CO_2-brine-quartz system and found much larger CA which is inconsistent to our results. According to their research, the impact caused by pollution is contrary to our results. Wang et al. [29] illustrated adhesion was most widely observed on extremely smooth surfaces with roughness on the order of ~10 nanometers. According to hypothesis based on DLVO theory, the thickness of brine film plays an importance role in adhesion. On smoother surface, the wet phase is less likely to accumulate in surface asperities and water film is easier to get rid of during CO_2 expansion, thus adhesion happens. Large hysteresis was found in all the four positions in set 7. If the mechanism of large hysteresis is adhesion, rather than saying that adhesion happens by accident, it can be said that the occurrence of adhesion is common. Despite large

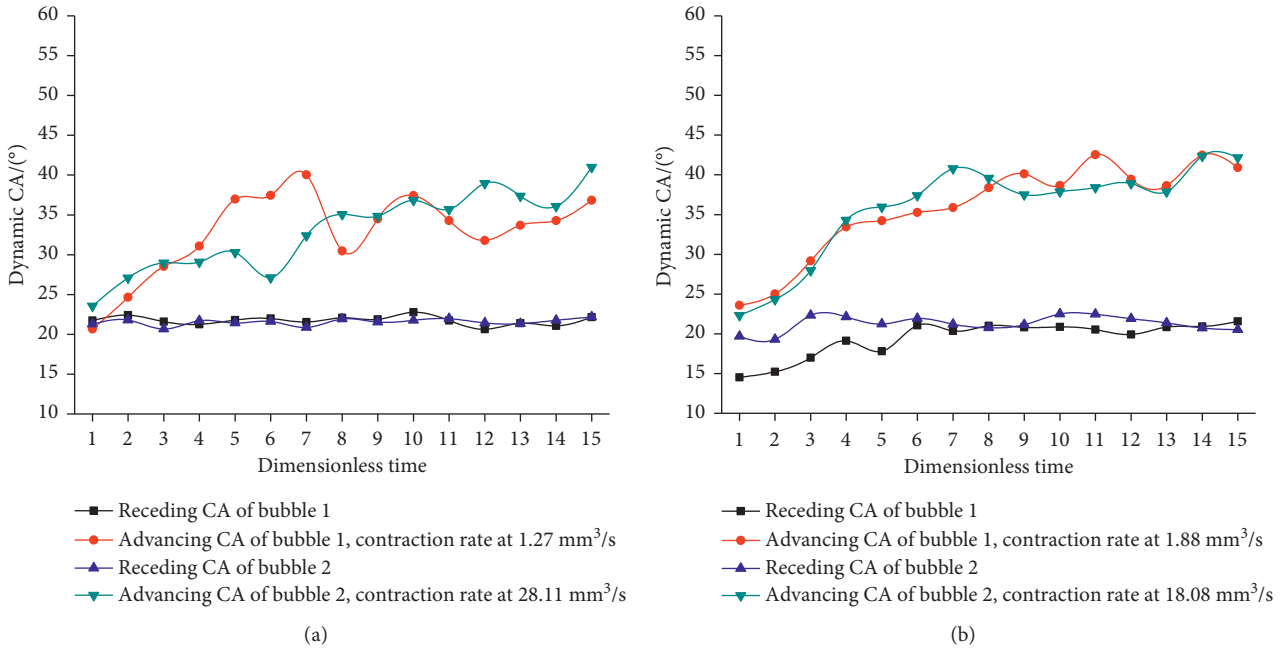

Figure 13: Advancing CA of contraction rates at 1 mol/L NaCl and 45°C. The pressure of left and right figures is 8 and 12 MPa, respectively. Tests of each experiment were conducted at the same surface area with timespan less than 0.5 h.

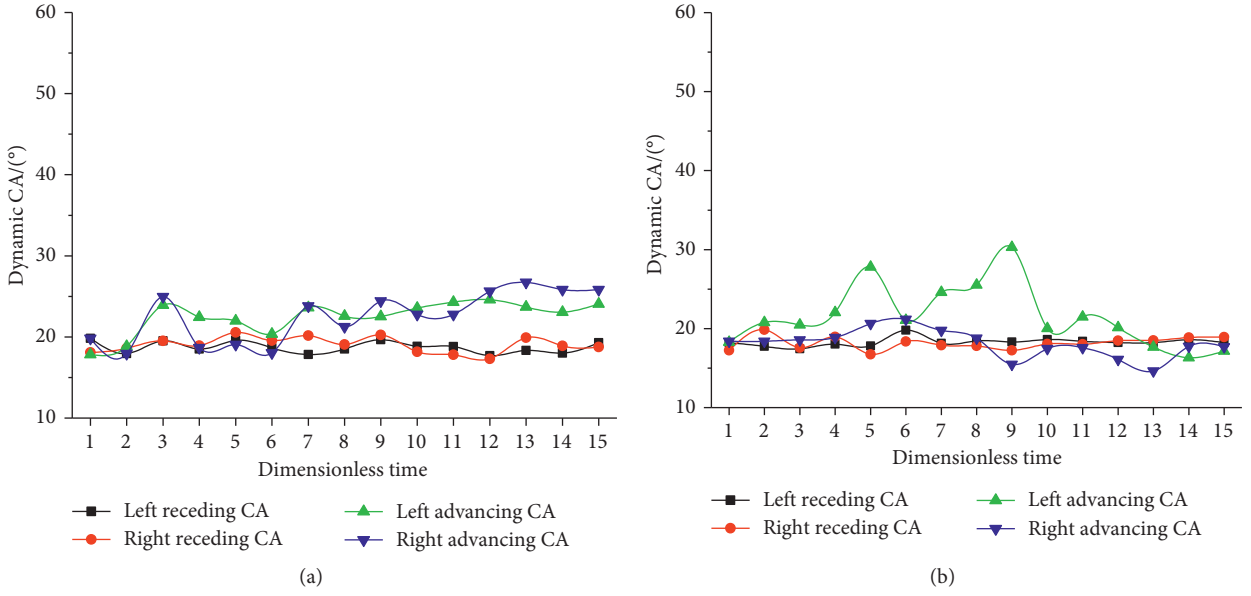

Figure 14: Dynamic results of experiment set 2 at position ② at 12 MPa, 1 mol/L NaCl, and 45°C. The measure time of dynamic tests of left and right figures is 15 : 30 and 18 : 30, respectively.

deviation in dynamic tests, repeated tests on the same position were similar and position depended dynamic characteristics (contact line pinning and leap) were observed; also, the same sets of dynamic experiments with fewer uncertainties have smaller deviations, so partial surface properties may be the key factor for adhesion, and randomness of adhesion may due to surface heterogeneity. Here, electron microscope tests illustrate that large hysteresis is related with smoother surface, supporting the DLVO-based adhesion hypothesis concerning about water film thickness, while other factors may also account for the hysteresis. Molecular simulation [45] also showed that the CA phenomenon is strongly affected by the presence of thin liquid films: CA increased with decreased film thickness and on mediate hydrophilic surfaces (Q^3), water films were absent when CO_2 droplets directly contact with the surfaces implying a film rupture mechanism for CO_2 adhesion on hydrated

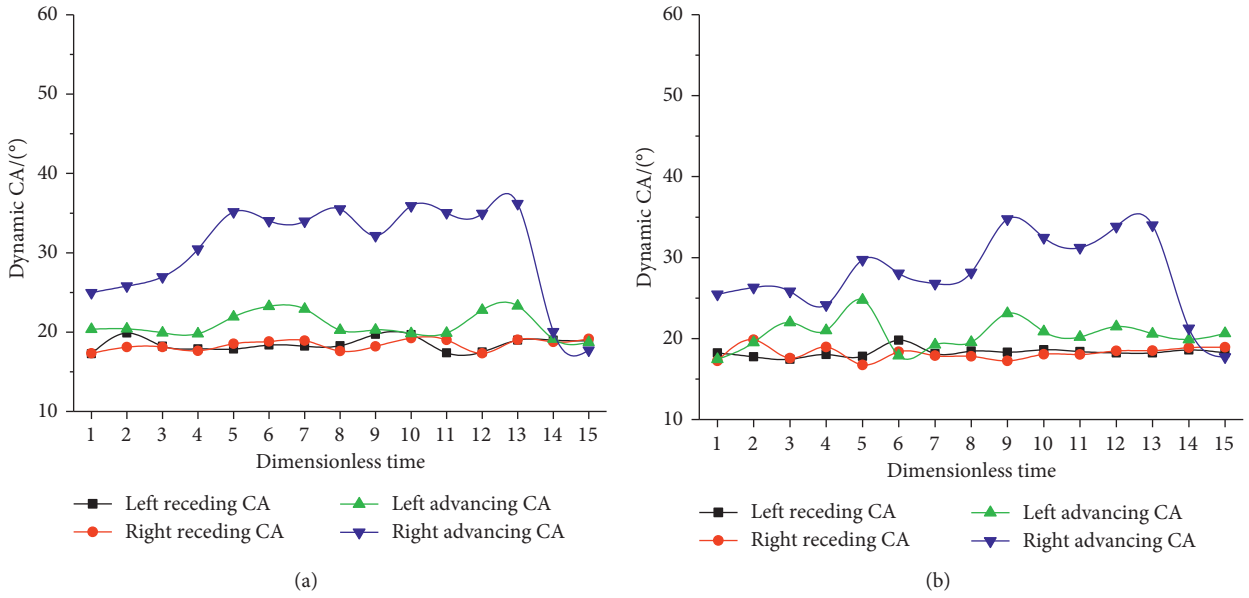

Figure 15: Dynamic results of experiment set 2 at position ③ at 12 MPa, 1 mol/L NaCl, and 45°C. The measure time of dynamic tests of left and right figures is 15 : 45 and 18 : 15, respectively.

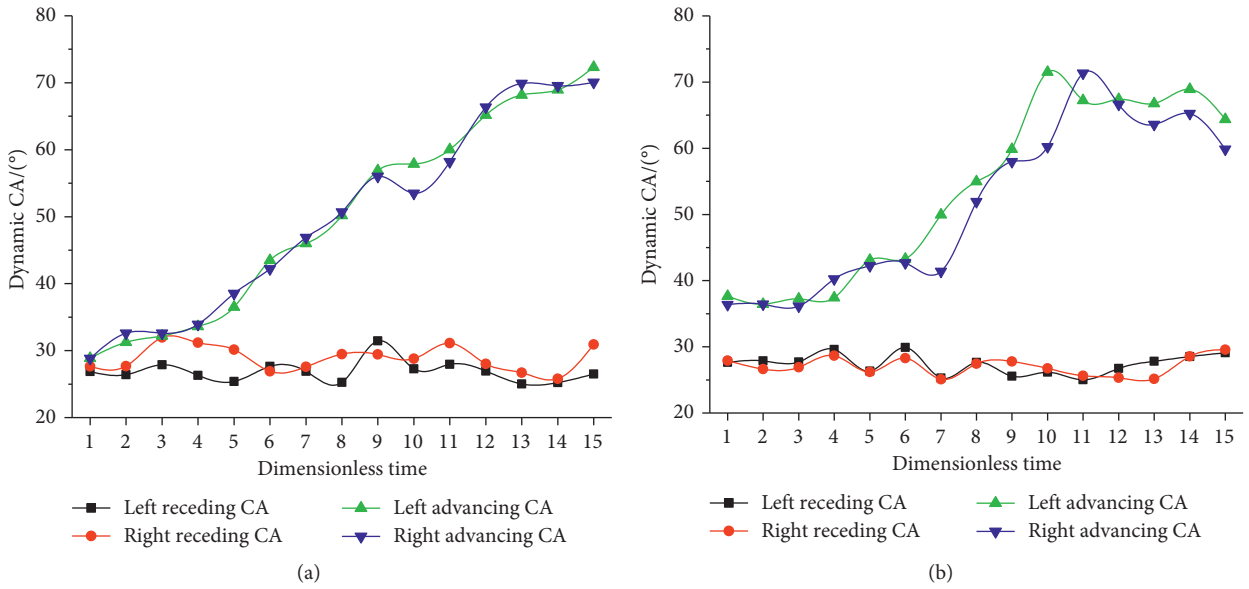

Figure 16: Dynamic results of experiment set 7 at position ① at 12 MPa, 1 mol/L NaCl, and 45°C. The measure time of dynamic tests of left and right figures is 17 : 00 and 19 : 50, respectively.

mineral surfaces. Microscope images of newly cleaved surface were similar with set 7. Dots can be seen in the left image, and the right-side surface is pure enough to find only two dots. Since the muscovite for electron microscope needs to be sprayed with platinum, the surface changes of the sample after the experiment cannot be obtained. Also, because of the large magnification, it is difficult to align the scanning area with the dynamic experimental area. From EDS results, the element composition of the three samples is similar.

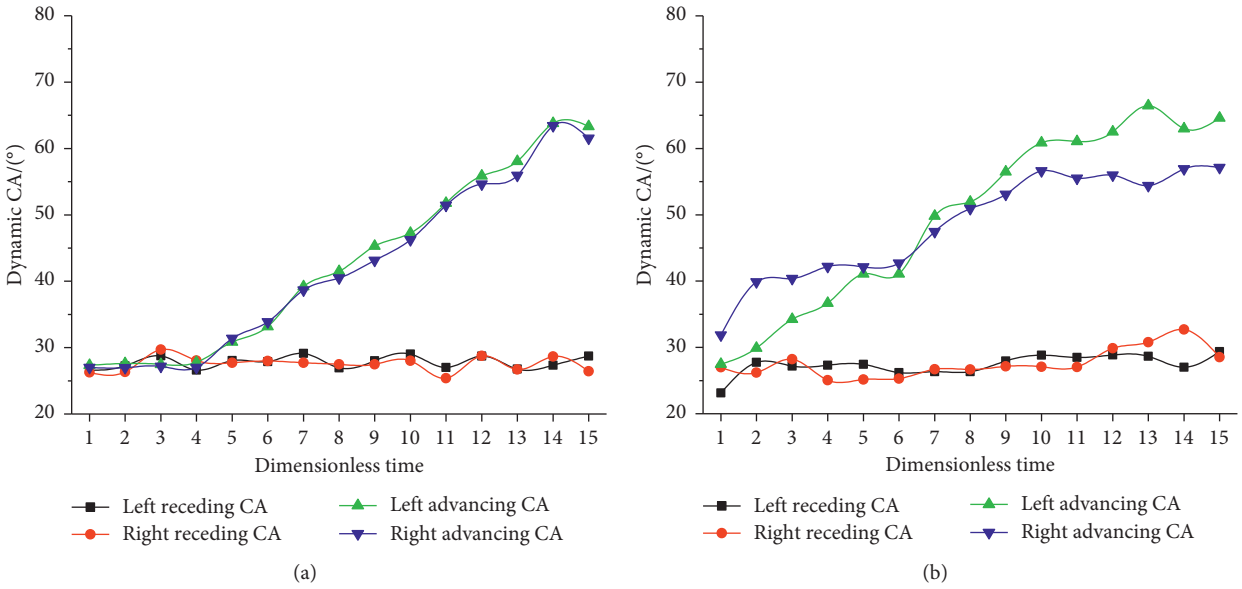

Figure 17: Dynamic results of experiment set 8 at position ① at 12 MPa, 1 mol/L NaCl, and 45°C. The measure time of dynamic tests of left and right figures is 17 : 15 and 19 : 50, respectively.

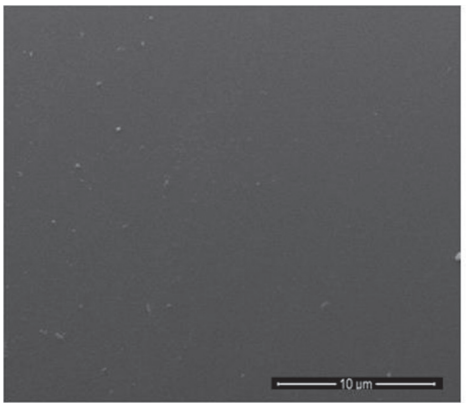

Element	Mole fraction
C	12.08
O	59.46
Na	0.38
Mg	0.31
Al	11.09
Si	13.08
K	3.25
Fe	0.35

Figure 18: Electron microscope (10000X magnification) of muscovite after experiment in set 4 and EDS results.

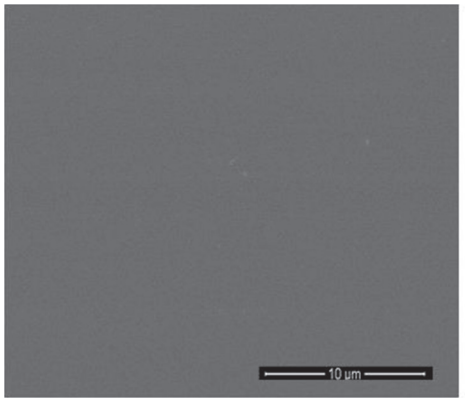

Element	Mole fraction
C	12.34
O	58.85
Na	0.39
Mg	0.46
Al	10.94
Si	13.17
K	3.34
Ti	0.12
Fe	0.39

Figure 19: Electron microscope (10000X magnification) of muscovite after experiment in set 7 and EDS results.

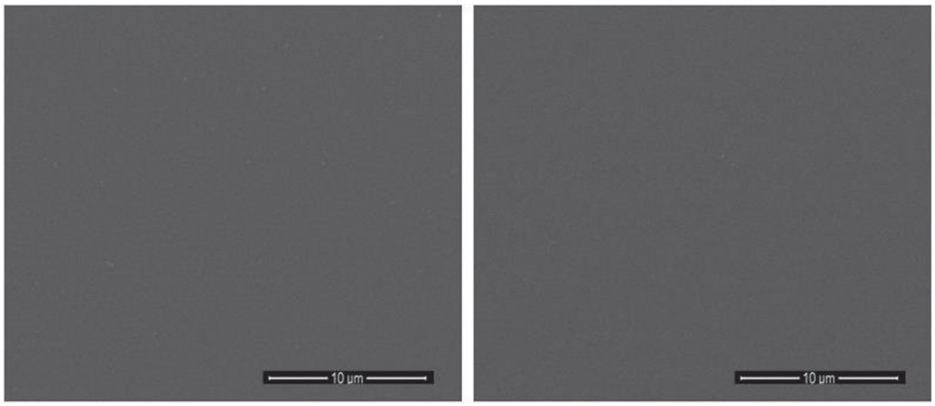

Element	Mole fraction
C	11.46
O	58.13
Na	0.34
Mg	0.32
Al	11.62
Si	13.97
K	3.71
Fe	0.45

Figure 20: Electron microscope (10000X magnification) of muscovite after experiment in set 7 and EDS results.

4. Conclusions

In the present study, we conducted static and dynamic contact angle tests for CO_2/brine/mica system under a wide range of pressures, temperatures, and salinities. In all static tests, both muscovite and phlogopite show hydrophilic property while bubbles of different CA on left and right sides were found. The average static CA ranges from 19.5° to 32.1°. In 8 MPa experiments, CA decreases from 26.0° to 19.5° with the increasing salinity. Similar trends were also observed under 12 MPa condition. Analysis of bubble movement during static tests explains the correlation between this phenomenon and CA hysteresis in dynamic tests. In dynamic CA tests, we conducted repeated tests on muscovite surface under 12 MPa, 45°C, and 1 mol/NaCl condition to explore effects of adhesion. Uncertainty and large hysteresis of dynamic results were found. By excluding multiple possible influencing factors, we found both uncertainty and hysteresis were related to measurement position, in other words surface physicochemical heterogeneity. Large hysteresis as obvious sign of adhesion had good repeatability at specific surface positions. Further electron microscope test demonstrated the correlation between large hysteresis and smoother surfaces which is consistent with the DLVO theory-based water film thickness hypothesis on adhesion. This study enriched the data on the wettability of mica and analyzed the uncertainty in the wettability measurement. In future research, it is necessary to explore the wettability of true heterogeneous geological storage environment.

Data Availability

All the data used to support the findings of this study are included within the article.

Conflicts of Interest

The authors declare that they have no conflicts of interest.

Acknowledgments

This research was supported by the National Natural Science Foundation of China (52076032), National Key Research and Development Project (2019YFC0312304), and Fundamental Research Funds for the Central Universities (DUT21LAB121).

References

[1] S. Bachu, "Sequestration of CO_2 in geological media: criteria and approach for site selection in response to climate change," *Energy Conversion and Management*, vol. 41, no. 9, pp. 953–970, 2000.

[2] S. Bachu and J. J. Adams, "Sequestration of CO_2 in geological media in response to climate change: capacity of deep saline aquifers to sequester CO_2 in solution," *Energy Conversion and Management*, vol. 44, no. 20, pp. 3151–3175, 2003.

[3] S. Saira, H. Yin, and F. Le-Hussain, "Effect of alcohol-treated CO_2 on interfacial tension between CO_2 and oil, and oil swelling," *Advances in Geo-Energy Research*, vol. 5, no. 4, pp. 407–421, 2021.

[4] Z. Kou, H. Wang, V. Alvarado, J. F. McLaughlin, and S. A. Quillinan, "Impact of sub-core scale heterogeneity on CO_2/brine multiphase flow for geological carbon storage in the upper Minnelusa sandstones," *Journal of Hydrology*, vol. 599, 2021.

[5] Z. Kou, D. Zhang, Z. Chen, and Y. Xie, "Quantitatively determine CO_2 geosequestration capacity in depleted shale reservoir: a model considering viscous flow, diffusion, and adsorption," *Fuel*, vol. 309, 2022.

[6] Z. Kou, T. Wang, Z. Chen, and J. Jiang, "A fast and reliable methodology to evaluate maximum CO_2 storage capacity of depleted coal seams: a case study," *Energy*, vol. 231, 2021.

[7] H. Wang, Z. Kou, J. Guo, and Z. Chen, "A semi-analytical model for the transient pressure behaviors of a multiple fractured well in a coal seam gas reservoir," *Journal of Petroleum Science and Engineering*, vol. 198, 2021.

[8] L. Zhang, Z. Kou, H. Wang et al., "Performance analysis for a model of a multi-wing hydraulically fractured vertical well in a coalbed methane gas reservoir," *Journal of Petroleum Science and Engineering*, vol. 166, pp. 104–120, 2018.

[9] M. A. Hesse, F. M. Orr, and H. A. Tchelepi, "Gravity currents with residual trapping," *Journal of Fluid Mechanics*, vol. 611, pp. 35–60, 2008.

[10] J. M. Ketzer, R. S. Iglesias, and S. Einloft, "Reducing greenhouse gas emissions with CO_2 capture and geological storage," *Handbook of Climate Change Mitigation*, Springer, New York, NY, USA, 2012.

[11] S. Iglauer, "Dissolution trapping of carbon dioxide in reservoir formation brine-a carbon storage mechanism," *Open Access Peer-Reviewed Chapter*, IntechOpen, Queensland, Australia, 2011.

[12] S. Iglauer, A. Paluszny, C. H. Pentland, and M. J. Blunt, "Residual CO_2 imaged with X-ray micro-tomography," *Geophysical Research Letters*, vol. 38, 2011.

[13] R. Juanes, E. J. Spiteri, F. M. Orr, and M. J. Blunt, "Impact of relative permeability hysteresis on geological CO_2 storage," *Water Resources Research*, vol. 42, 2006.

[14] A. Raza, R. Rezaee, R. Gholami et al., "Injectivity and quantification of capillary trapping for CO_2 storage: a review of influencing parameters," *Journal of Natural Gas Science and Engineering*, vol. 26, pp. 510–517, 2015.

[15] S. Iglauer, W. Wülling, C. H. Pentland, S. K. Al-Mansoori, and M. J. Blunt, "Capillary-trapping capacity of sandstones and sandpacks," *Spe Journal*, vol. 16, no. 4, pp. 778–783, 2011c.

[16] E. Lindeberg and D. Wessel-Berg, "Vertical convection in an aquifer column under a gas cap of CO_2," *Energy Conversion and Management*, vol. 38, pp. S229–S234, 1997.

[17] I. Gaus, "Role and impact of CO_2-rock interactions during CO_2 storage in sedimentary rocks," *International Journal of Greenhouse Gas Control*, vol. 4, no. 1, pp. 73–89, 2010.

[18] S. Iglauer, A. Z. Al-Yaseri, R. Rezaee, and M. Lebedev, "CO_2 wettability of caprocks: implications for structural storage capacity and containment security," *Geophysical Research Letters*, vol. 42, no. 21, pp. 9279–9284, 2015a.

[19] A. A.-Y. Stefan Iglauer, "Improving basalt wettability to de-risk CO_2 geo-storage in basaltic formations," *Advances in Geo-Energy Research*, vol. 5, no. 3, pp. 347–350, 2021.

[20] T. K. Tokunaga and J. M. Wan, "Capillary pressure and mineral wettability influences on reservoir CO_2 capacity," *Geochemistry of Geologic CO_2 Sequestration*, vol. 77, pp. 481–503, 2013.

[21] E. A. Al-Khdheeawi, S. Vialle, A. Barifcani, M. Sarmadivaleh, and S. Iglauer, "Effect of wettability heterogeneity and reservoir temperature on CO_2 storage efficiency in deep saline aquifers," *International Journal of Greenhouse Gas Control*, vol. 68, pp. 216–229, 2018.

[22] S. Iglauer, C. H. Pentland, and A. Busch, "CO_2 wettability of seal and reservoir rocks and the implications for carbon geo-sequestration," *Water Resources Research*, vol. 51, no. 1, pp. 729–774, 2015.

[23] M. Arif, A. Z. Al-Yaseri, A. Barifcani, M. Lebedev, and S. Iglauer, "Impact of pressure and temperature on CO_2 -brine-mica contact angles and CO_2 -brine interfacial tension: implications for carbon geo-sequestration," *Journal of Colloid and Interface Science*, vol. 462, pp. 208–215, 2016.

[24] D. Broseta, N. Tonnet, and V. Shah, "Are rocks still water-wet in the presence of dense CO_2 or H2S?" *Geofluids*, vol. 12, no. 4, pp. 280–294, 2012.

[25] P. Chiquet, D. Broseta, and S. Thibeau, "Wettability alteration of caprock minerals by carbon dioxide," *Geofluids*, vol. 7, no. 2, pp. 112–122, 2007.

[26] R. Farokhpoor, B. J. A. Bjørkvik, E. Lindeberg, and O. Torsæter, "Wettability behaviour of CO_2 at storage conditions," *International Journal of Greenhouse Gas Control*, vol. 12, pp. 18–25, 2013.

[27] J. M. Wan, Y. Kim, and T. K. Tokunaga, "Contact angle measurement ambiguity in supercritical CO_2-water-mineral systems: mica as an example," *International Journal of Greenhouse Gas Control*, vol. 31, pp. 128–137, 2014.

[28] S. B. Wang, I. M. Edwards, and A. F. Clarens, "Wettability phenomena at the CO_2-brine-mineral interface: implications for geologic carbon sequestration," *Environmental Science & Technology*, vol. 47, pp. 234–241, 2013a.

[29] S. B. Wang, Z. Y. Tao, S. M. Persily, and A. F. Clarens, "CO_2 adhesion on hydrated mineral surfaces," *Environmental Science & Technology*, vol. 47, pp. 11858–11865, 2013b.

[30] M. Arif, A. Barifcani, M. Lebedev, and S. Iglauer, "Structural trapping capacity of oil-wet caprock as a function of pressure, temperature and salinity," *International Journal of Greenhouse Gas Control*, vol. 50, pp. 112–120, 2016.

[31] M. Jafari and J. Jung, "Variation of contact angles in brine/CO_2/mica system considering short-term geological CO_2 sequestration condition," *Geofluids*, vol. 2018, Article ID 3501459, 15 pages, 2018.

[32] S.-J. Hong, F.-M. Chang, T.-H. Chou, S. H. Chan, Y.-J. Sheng, and H.-K. Tsao, "Anomalous contact angle hysteresis of a captive bubble: advancing contact line pinning," *Langmuir*, vol. 27, no. 11, pp. 6890–6896, 2011.

[33] A. Carre and V. Lacarriere, "Study of surface charge properties of minerals and surface-modified substrates by wettability measurements," *Contact Angle, Wettability and Adhesion*, vol. 4, p. 267, 2006.

[34] J. S. Buckley, "Effective wettability of minerals exposed to crude oil," *Current Opinion in Colloid & Interface Science*, vol. 6, no. 3, pp. 191–196, 2001.

[35] J. S. Buckley, K. Takamura, and N. R. Morrow, "Influence of electrical surface charges on the wetting properties of crude oils," *SPE Reservoir Engineering*, vol. 4, no. 3, pp. 332–340, 1989.

[36] N. R. Morrow, H. T. Lim, and J. S. Ward, "Effect of crude-oil-induced wettability changes on oil recovery," *SPE Formation Evaluation*, vol. 1, no. 1, pp. 89–103, 1986.

[37] T. W. Kim, T. K. Tokunaga, J. R. Bargar, M. J. Latimer, and S. M. Webb, "Brine film thicknesses on mica surfaces under geologic CO_2 sequestration conditions and controlled capillary pressures," *Water Resources Research*, vol. 49, no. 8, pp. 5071–5076, 2013.

[38] J.-W. Jung and J. Wan, "Supercritical CO_2 and ionic strength effects on wettability of silica surfaces: equilibrium contact angle measurements," *Energy & Fuels*, vol. 26, no. 9, pp. 6053–6059, 2012.

[39] A. F. Stalder, T. Melchior, M. Muller, D. Sage, T. Blu, and M. Unser, "Low-bond axisymmetric drop shape analysis for surface tension and contact angle measurements of sessile drops," *Colloids and Surfaces A-Physicochemical and Engineering Aspects*, vol. 364, pp. 72–81, 2010.

[40] S. Saraji, L. Goual, M. Piri, and H. Plancher, "Wettability of supercritical carbon dioxide/water/quartz systems: simultaneous measurement of contact angle and interfacial tension at reservoir conditions," *Langmuir*, vol. 29, pp. 6856–6866, 2013.

[41] Z. Adamczyk, M. Zaucha, and M. Zembala, "Zeta potential of mica covered by colloid particles: a streaming potential study," *Langmuir*, vol. 26, no. 12, pp. 9368–9377, 2010.

[42] A. Kaya and Y. Yukselen, "Zeta potential of clay minerals and quartz contaminated by heavy metals," *Canadian Geotechnical Journal*, vol. 42, no. 5, pp. 1280–1289, 2005.

[43] J. N. Israelachvili, "Intermolecular and surface forces," *With Applications to Colloidal and Biological Systems*, Elsevier, Amsterdam, Netherlands, 2011.

[44] S. Iglauer, A. Salamah, M. Sarmadivaleh, K. Liu, and C. Phan, "Contamination of silica surfaces: impact on water-CO_2-quartz and glass contact angle measurements," *International Journal of Greenhouse Gas Control*, vol. 22, pp. 325–328, 2014.

[45] W. Hu, C. Chen, W. Li, and Y. Song, "Interrelationship between water film thicknesses and contact angles and a model for CO_2 adhesion," *Molecular Simulation*, vol. 45, no. 11, pp. 868–875, 2019.